ELSEVIER

Contents lists available at ScienceDirect

# Earth and Planetary Science Letters

www.elsevier.com/locate/epsl



# Reconciling chemical weathering rates across scales: Application of uranium-series isotope systematics in volcanic weathering clasts from Basse-Terre Island (French Guadeloupe)



Jiye Guo<sup>a,\*</sup>, Lin Ma<sup>a,\*</sup>, Jerome Gaillardet<sup>b</sup>, Peter B. Sak<sup>c</sup>, Yvette Pereyra<sup>a</sup>, Jacqueline Engel<sup>a</sup>

- <sup>a</sup> Department of Geological Sciences, University of Texas at El Paso, El Paso, TX 79968, USA
- <sup>b</sup> Université de Paris, Institut de physique du globe de Paris, CNRS, F-75005 Paris, France
- <sup>c</sup> Department of Earth Sciences, Dickinson College, Carlisle, PA 17013, USA

#### ARTICLE INFO

# Article history: Received 15 March 2019 Received in revised form 30 August 2019 Accepted 28 September 2019 Available online 23 October 2019 Editor: I. Halevy

Keywords: U-series isotopes weathering rates weathering clasts river weathering fluxes French Guadeloupe

#### ABSTRACT

To elucidate the factors that contribute to the orders of magnitude difference generally observed in apparent weathering rates across scales, we utilized a U-series isotopic technique to directly determine the duration and rates of chemical weathering recorded in weathering clasts. In this study, we systematically compiled 15 individual volcanic weathering clasts collected from eight andesitic watersheds along a gradient of mean annual precipitation ranging from  $\sim$ 1600 mm to 6400 mm on the tropical volcanic Basse-Terre Island of French Guadeloupe. We measured U-series isotope compositions to quantify weathering advance rates along the core-rind transects in these weathering clasts. Total rind formation ages, the length of time it took for these weathering clasts to form from andesitic rock fragments or volcanic clasts in the soil zones, range from 60 kyr to 300 kyr. As expected for each individual core-rind weathering transect, the rind ages generally increase almost linearly with distance away from the core-rind boundary. The derived clast weathering rates range from 0.08  $\pm$  0.04 to 0.34  $\pm$  0.01 mm kyr<sup>-1</sup>, and the rates exhibit a strong positive correlation ( $R^2 = 0.74$ ) with the annual runoff values of these watersheds. This correlation documents the first direct evidence that weathering over geological timescales on the island is controlled by the amount of precipitation and corroborates the relationship that was previously reported for the riverine weathering fluxes at Basse-Terre Island in Guadeloupe, but measured with much shorter time scales. The clast-scale rates (inferred for the characteristic length scale of mm) are compared to the watershed-scale rates of Basse-Terre Island (length scale of km): constantly higher rates are observed at the watershed scales than the clast scale and the discrepancy equals  $\sim$ 1800  $\pm$  400 times, despite changes in watershed characteristics such as watershed size, relief, and runoff values. The discrepancy is attributed to the fractal nature of the roughness and surface area across scales. For example, the presence of undulations and fractures (e.g. roughness) at the bedrock-saprolite contact of the watershed, which is generally not assessed in the watershed surface area estimates, is most likely the main contributor to the constant rate difference of  $\sim$ 1800 times.

© 2019 Elsevier B.V. All rights reserved.

# 1. Introduction

Chemical weathering of volcanic rocks, i.e. the neutralization and release of base cations by carbonic and sulfuric acids, is one of the most fundamental and important process at Earth's surface, impacting Earth systems by consuming atmospheric CO<sub>2</sub> and creating important solute fluxes to the ocean and ecosystems (e.g., Gaillardet et al., 1999; Vitousek et al., 1999; Dessert et al., 2003).

Understanding the mechanistic controls of volcanic rock weathering is thus a fundamental research question in Earth System Science. Accurate measurement of the weathering rates, i.e., the reaction kinetics between water and minerals in the Critical Zone (e.g., Brantley et al., 2006), is necessary to investigate the potential feedbacks among weathering and erosion of volcanic rocks, land-scape, climate, hydrology, ecosystem, and tectonic regime (Brantley et al., 2008; Oelkers and Schott, 2009). A number of methods and approaches have been used to determine weathering rates. For example, weathering rates can be quantified using river chemistry as "integrators" of chemical fluxes from watersheds, chem-

<sup>\*</sup> Corresponding authors.

E-mail addresses: jguo2@miners.utep.edu (J. Guo), lma@utep.edu (L. Ma).

ical and isotopic compositions of solid weathering products such as sediments, soil and regolith profiles, laboratory dissolution experiments, and reactive transport models (Brantley et al., 2008; Oelkers and Schott, 2009). However, weathering rates that are measured across a range of spatial and temporal scales generally differ by 2 to 5 orders of magnitude (White and Brantley, 2003; Navarre-Sitchler and Brantley, 2007). This discrepancy has been attributed to the fact that many of those rates were measured under intrinsically different conditions including surface roughness, reactive surface areas, erosional regimes, parent lithology, climate, conditions of fluid flows and residence times, and biological controls (Bluth and Kump, 1994; Drever and Stillings, 1997; Maher et al., 2004; 2010; Dupre et al., 2003; Anderson, 2005; West et al., 2005), hampering a direct comparison of weathering rates across scales. Independent measurements of weathering rates over a range of scales from the same study areas, e.g., from weathering clasts to soil profiles and to watersheds, are rarely reported and compared. Hence, very few studies have attempted to reconcile and elucidate the controls on the different weathering rates across scales (e.g., Navarre-Sitchler and Brantley, 2007; Jung and Navarre-Sitchler. 2018).

To investigate the factors contributing to the large difference in weathering rates across scales, we utilize a U-series isotopic technique for weathering clasts (Pelt et al., 2008; Ma et al., 2012) that facilitates the direct determination of the duration and rates of chemical weathering in solid weathering products. Useries isotopes in weathering products have shown great potential for quantifying rates of chemical weathering, erosion, and transport with timescales less than  $\sim$ 1.25 Ma (e.g., Sarin et al., 1990; Vigier et al., 2001; Dequincey et al., 2002; Maher et al., 2004; Krishnaswami et al., 2004; DePaolo et al., 2006; Dosseto et al., 2008; Pelt et al., 2008; Bourdon et al., 2009; Ma et al., 2010, 2012). The technique relies on U-series isotope disequilibrium that results from U-series fractionation due to different decay half-lives and geochemical properties (e.g., Ivanovich and Harmon, 1992; Bourdon et al., 2003). Mobility behavior of U-series isotopes (e.g.,  $^{238}$ U,  $^{234}$ U,  $^{230}$ Th, and  $^{232}$ Th) during low temperature water-rock interactions at weathering interfaces, soil profiles, or watersheds have been studied extensively (e.g., Chabaux et al., 2003; Dosseto et al., 2008), enabling the use of U-series isotopes in weathering clasts as a geochronometer (Pelt et al., 2008; Ma et al., 2012).

In this study, we focus on 15 individual volcanic weathering clasts collected from 8 andesitic watersheds along a gradient of mean annual precipitation ranging from ~1600 mm to 6400 mm on the tropical volcanic Basse-Terre Island of French Guadeloupe. Basse-Terre Island is a suitable field location to study chemical weathering due to its well-defined environmental gradients including climate, relief, and bedrock ages. In the tropical and thick volcanic soil profiles of Basse-Terre Island, partially weathered rock fragments or volcanic clasts are commonly present. These weathering clasts develop a rind of permeable and altered weathering products that envelops an unweathered core. Weathering clasts provide valuable samples to study the initiation and duration of chemical weathering in field systems (e.g., Cernohouz and Solc, 1966; Porter, 1975; Colman and Pierce, 1981; Sak et al., 2010), due to the presence of an easily identified corerind boundary and the apparent absence of physical erosion during rind formation. We measured U-series isotope compositions to quantify weathering advance rates of the core-rind boundary in these 15 weathering clasts, which represent weathering rates measured at the clast scale (with a characteristic length scale of mm). In contrast to previous studies of weathering clasts in which only one or two clasts from a single watershed were characterized, this study for the first time investigated systematically a large number of weathering clasts from multiple watersheds along a precipitation gradient. The compilation of rind weathering rates allows for

a direct comparison to the river chemical fluxes of Basse-Terre Island (length scale of km; Gaillardet et al., 2011). The two sets of independently determined weathering rates at two different field spatial and temporal scales offer insights to reconcile the rate difference observed in the multiple watersheds of the island.

#### 2. Background

#### 2.1. Basse-Terre Island

Basse-Terre Island is a part of the Guadeloupe archipelago, Lesser Antilles, with a surface area of  $850~\rm km^2$  (Fig. 1a). This island encompasses many small ( $<\sim 10~\rm km^2$ ) watersheds developed on similar andesitic volcanic rocks. Superimposed on this compositionally similar bedrock are strong gradients in bedrock ages, relief, and precipitation (Fig. 1).

To study the impacts of steep environmental gradients on the dynamics of surface processes including landslides, floods, river fluxes, and sediment transport, Basse-Terre Island was designated and managed as the Observatory of Erosion in Antilles by the Institut de Physique du Globe de Paris (IPGP). The observatory is a part of the international Critical Zone Exploration Network (CZEN) and the French CZO network (OZCAR; Gaillardet et al., 2018) and has been extensively studied for understanding chemical weathering and Earth surface processes, in additional to the potential natural hazards by active volcanism (Dessert et al., 2003, 2015; Chatanantavet et al., 2010; Sak et al., 2010, 2018; Gaillardet et al., 2011; Lloret et al., 2011; Ma et al., 2012, 2018; Allemand et al., 2014; Engel et al., 2016). In particular, two of the watersheds investigated in this study (Bras David and Capesterre; Fig. 1d) have been extensively monitored and investigated by the OBSERA Critical Zone Observatory (PI E. Lajeunesse), as a part of the French CZO network (Gaillardet et al., 2018).

Basse-Terre Island is comprised of relatively homogeneous andesitic to basaltic-andesitic volcanic materials such as lava flows, lava domes and pyroclastic deposits (e.g., Jordan, 1975; Hawkesworth and Powell, 1980; Samper et al., 2007). Bedrock ages decrease systematically from north to south (2.8 Ma to present) along the long axis of the island (Samper et al., 2007; Fig. 1b). The topography of the island reflects the patterns of bedrock ages, with high relief and steep slopes in the young and volcanic active southern area and lower relief and gentler slopes in the older and more stable northern part (Fig. 1c). Basse-Terre Island is characterized by a tropical and humid climate (Dessert et al., 2015). The topographic divide generates a strong pattern of orographic precipitation (MAP:  $\sim$ 1000 mm to >6000 mm) on Basse-Terre Island. Notably, the east and south coast receives high precipitation and the leeward west and north coast generally receives less precipitation (Fig. 1c). The variations of mean air temperatures are more limited (16-25 °C); only the high elevation areas in southern central island experience MAT <20 °C (Fig. 1c).

# 2.2. Short-term chemical weathering fluxes at watershed scale

The rivers on Basse-Terre Island transport a substantial load of solutes and sediments, among the highest fluxes found on Earth (Lloret et al., 2011; Gaillardet et al., 2011; Dessert et al., 2015). Chemical weathering fluxes of 28 major rivers on the island (40-430 t/km² watershed/yr), calculated based on the concentrations of rock-derived solutes multiplied by runoff, show a strong correlation with annual watershed runoff values (Gaillardet et al., 2011), indicating that the solute concentrations in rivers are not purely diluted by the addition of water during high runoffs, but rather that solute concentrations remain relatively constant across the Island for a suite of watersheds with highly variable magnitudes of runoff. The relative constancy of concentrations

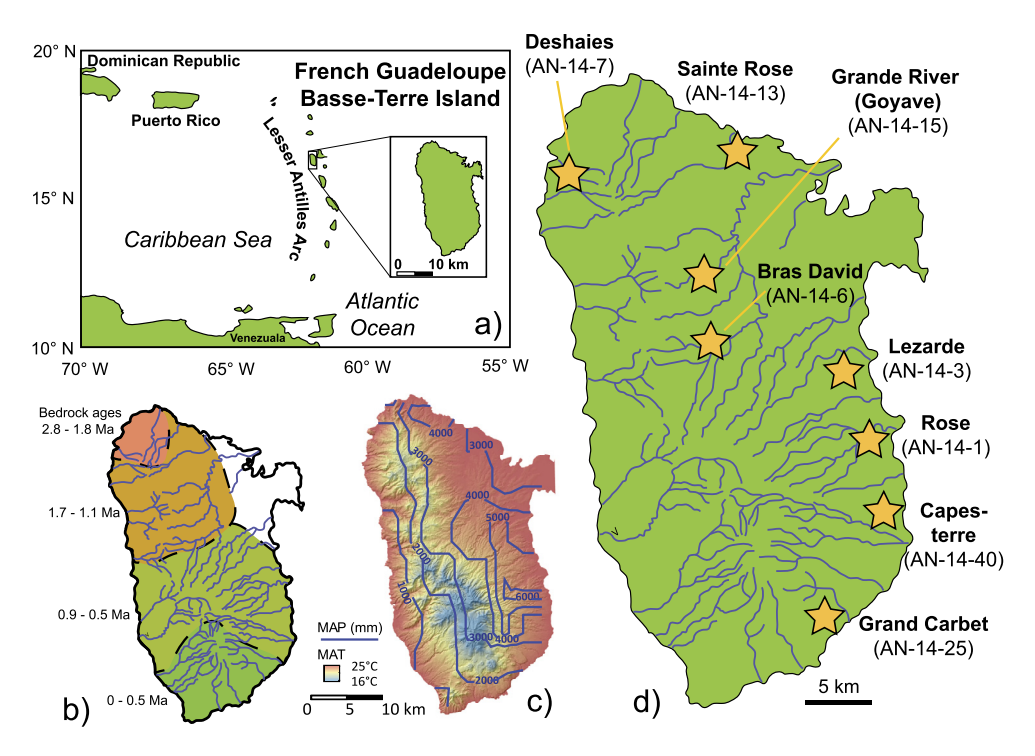


**Fig. 1. a)** Location map of Basse-Terre Island (French Guadeloupe); Major geographic features in the Caribbean region are shown; **b)** Distribution of bedrock ages (Myr) on Basse-Terre Island (Samper et al., 2007); **c)** Contours of mean annual precipitation (MAP: mmyr<sup>-1</sup>; NASA TRMM data; https://pmm.nasa.gov/trmm) and color map of mean annual temperature (MAT: °C); Shaded topographic map of Basse-Terre Island is in the background; **d)** Major rivers and watersheds on Basse-Terre Island; Clast sampling locations in this study are shown as stars. (For interpretation of the colors in the figure(s), the reader is referred to the web version of this article.)

in rivers despite of large temporal runoff variations is classically observed as the chemostatic effect (e.g., Godsey et al., 2009; Gislason et al., 2009). In the Lesser Antilles, Gaillardet et al. (2011) reported that the total dissolved solute of rivers (TDS: mg/L) varies as a function of runoff (R: mm/yr): TDS = 590 R $^{-0.4}$  where the exponent of -0.4 (>-1) indicates increased chemical weathering at high runoff compensates for water dilution. Therefore, the watershed-based fluxes (calculated by TDS  $\times$  R) increase positively with runoff (R).

As orographic effect exerts a first order control on runoff across the island of Basse-Terre, Gaillardet et al. (2011) proposed that volcanic activity on Basse-Terre could exert a negative feedback on atmospheric CO2 levels. For example, volcanic activity creates relief and promotes high amounts of orographic precipitation and relatively permeable infiltration regimes; these factors then result in elevated chemical weathering fluxes and atmospheric CO<sub>2</sub> consumption. The accelerated weathering of silicate rocks and associated CO2 drawdown triggered by volcanic uplift could provide an important mechanism to regulate atmospheric CO2 concentration, in addition to the well-established temperature-related feedback mechanism (e.g., Walker et al., 1981; Berner et al., 1983). This hypothesis highlights the importance of the hydrologic cycle in controlling chemical weathering and CO2 consumption on volcanic islands (Godsey et al., 2009; Gaillardet et al., 2011) and the necessity to accurately constrain the relationship between solute concentration and runoff at the regional scale.

The chemical weathering fluxes calculated based on river chemistry are however contemporary with modern climate conditions. They do not necessarily reflect the establishment of the precipitation and relief patterns, for example at Basse-Terre Island, over geological timescales. Furthermore, the calculation of riverine weathering fluxes, as shown above, uses directly river runoff values and might create a mathematic complication to interpret the relationship observed between weathering fluxes and river runoff. One way to circumvent some of these complications is to measure chemical weathering rates in solid-state weathering products,

not only as an independent comparison to riverine fluxes, but also as an alternative approach to document the controls on chemical weathering over geologic timescales at a different spatial scale.

# 2.3. Weathering clasts and U-series systematics

Rock fragments in regolith commonly form alteration rinds. Compared to the unweathered parent core, the rind is enriched in relatively immobile elements (e.g. Ti, Fe, Th, and Al) and depleted in mobile elements (e.g. Mg, Ca, Na, and K) (e.g. Colman and Pierce, 1981; Sak et al., 2010). The presence of thick weathering rinds, i.e. rind material remaining in place around the core, suggests no significant physical erosion occurred to the weathering clasts. The easy-to-identify core-rind boundary marks the initial location for weathering to occur. The simplicity of a weathering rind system has led to several significant advances in the use of U-series systematics in weathering rinds to quantify rates and duration of chemical weathering. Specifically, rind formation rates have been successfully measured on a number of clasts from Costa Rica and Guadeloupe (Pelt et al., 2008; Ma et al., 2012, 2018; Engel et al., 2016; Sak et al., 2018). In those efforts, it was demonstrated that the behaviors of U-series isotopes during rind formation are well constrained in individual clasts and that the isotope mass balance approach (e.g. Dequincey et al., 2002; Ma et al., 2012; Dosseto et al., 2008) can be utilized as a reliable dating tool.

#### 3. Materials and methods

We compiled 15 weathering clasts collected from 8 watersheds on Basse-Terre Island along well-defined environmental gradients of bedrock ages, relief, and precipitation (Table 1). New analyses and characterization were conducted for 11 of the 15 samples in this study and results from previously published studies were compiled for the other 4 samples (Sak et al., 2010, 2018; Ma et al., 2012, 2018; Engel et al., 2016). The clast collection, preparation,

**Table 1**Information of the compiled 15 weathering clasts from the 8 watersheds of Basse-Terre Island, French Guadeloupe.

Site ID	Clast name	Watershed name	Latitude DD MM.MMM	Longitude DD MM.MMM	Relief <sup>a</sup> (m)	MAT <sup>b</sup> (°C)	MAP <sup>b</sup> (mm/yr)	Runoff <sup>a</sup> (mm/yr)	TWR <sup>a</sup> (ton/km <sup>2</sup> /yr)
AN-14-1	AN-14-1.6 AN-14-19.4 AN-14-19.6	Rose	16 07.845 N	61 35.861 W	1079	24.7	5280	2825	79
AN-14-3	AN-14-3.2° AN-14.3.5 AN-14-17.2	Lezarde	16 11.787 N	61 36.326 W	749	24.9	4520	3750	101
AN-14-6	Bras David	Bras David	16 10.508 N	61 41.746 W	972	23.3	3840	3000	92
AN-14-7	AN-14-7.5* AN-14-7.6*	Deshaies	16 18.635 N	61 46.601 W	465	23.2	1640	1000	46
AN-14-13	AN-14-13.1 AN-14-13.2	Sainte Rose	16 19.442 N	61 42.832 W	587	24.5	3810	1850	71
AN-14-15	AN-14-15.1	Grande Riv. at Goyave	16 13.856N	61 42.197 W		23.4	3150	2950	78
AN-14-25	AN-14-25.3	Grand Carbet	16 00.319 N	61 36.185 W	1220	20.0	4000	6000	427
AN-16-40	AN-16-40.1 AN-16-40.2	Capesterre	16 06.705 N	61 34.433 W	1132	24.8	6350	5200	181

- <sup>a</sup> Gaillardet et al. (2011); Relief refers to total watershed relief; TWR: total weathering rates from watersheds.
- b Tropical rainfall measuring mission (TRMM) data source: pmm.nasa.gov/trmm; MAT: mean annual temperature; MAP: mean annual precipitation.

and analytical methods were described in detail in the supplement materials (Appendix 1; Table A1). Major element concentrations and U-series isotope compositions of the weathering clast samples were measured on ICP-OES and MC-ICPMS at Penn State University and University of Texas at El Paso (UTEP), respectively.

#### 4. Results

# 4.1. Major element chemistry

All but one of the newly analyzed 11 clast samples in this study have unweathered cores in the center, similar to the 4 previously analyzed samples (Sak et al., 2010, 2018; Ma et al., 2012, 2018; Engel et al., 2016). Only sample AN-14-19.4 has been completely weathered with no core present (Fig. A1). Core compositions are all primarily andesitic (Ma, 2018). The dominant minerals in these cores are pyroxene, plagioclase, both as small phenocrysts (<1000  $\mu$ m, much smaller than the diameter of the drilled bit, 3.2 mm) and in fine groundmass matrix, volcanic glass materials, and minor phases such as ilmenite. These weathering clasts were developed from rock fragments or volcanic clasts within pyroclastic flows with major element compositions similar to other andesitic volcanic materials, e.g., lava flows or bedrock, on Basse-Terre Island (Samper et al., 2007).

The rind material is readily distinguishable from both the encasing soils and unweathered cores on the basis of color (Fig. A1). The core-rind boundary is sharp and abrupt with an increase in porosity, near the starting location for initial stage of core weathering. Relative to the core, the rind is significantly depleted in CaO, Na<sub>2</sub>O, MgO, K<sub>2</sub>O, and relatively enriched in SiO<sub>2</sub>, Al<sub>2</sub>O<sub>3</sub>, and Fe<sub>2</sub>O<sub>3</sub> (Ma, 2018). Such chemical changes across the core-rind boundary are consistent with the previously observed weathering reactions in weathering clasts from Basse-Terre Island: weathering of glass matrix, groundmass (fine crystals of plagioclase, pyroxene), and primary minerals (plagioclase, pyroxene) from the cores to produce Fe oxy-hydroxides, gibbsite and minor kaolinite in the rinds (Sak et al., 2010).

# *4.2. U-series systematics*

The unweathered cores of all the weathering clasts from Basse-Terre Island show average ( $^{234}$ U/ $^{238}$ U) = 1.018  $\pm$  0.031, ( $^{230}$ Th/ $^{238}$ U) = 0.972  $\pm$  0.042, and ( $^{230}$ Th/ $^{232}$ Th) = 1.002  $\pm$  0.048

(1SD, N=14; Table A2) and are generally in U-series equilibrium (i.e. U-series activity ratios =1), as expected with their emplacement ages older than 1 Ma. The U and Th elemental contents of these core samples show a relatively large range of values: 0.312 to 1.157 mg/Kg for U and 0.860 to 3.433 mg/Kg for Th. However, the core U/Th elemental ratios show limited variability, e.g. average ( $^{238}$ U/ $^{232}$ Th) ratio  $=1.032\pm0.064$  (1SD, N=14), consistent with the homogeneous U-series isotope signatures of the drilled core samples.

The rind materials of all of the weathering clasts show a clear signature of U series disequilibrium (Table A2) as evidenced by  $(^{234}\text{U}/^{238}\text{U})$  ratios (ranging from 0.964 to 1.071) and  $(^{230}\text{Th}/^{238}\text{U})$  ratios (ranging from 0.422 to 1.070), indicating that rind formation has disturbed the U-series equilibrium signatures. The U-series disequilibrium is also documented by variable and elevated  $(^{238}\text{U}/^{232}\text{Th})$  ratios in rind materials, ranging from 0.841 to 4.442, as compared to the average  $(^{238}\text{U}/^{232}\text{Th})$  ratio of 1.032 in the cores. Similarly, the rind materials are characterized by elevated  $(^{230}\text{Th}/^{232}\text{Th})$  ratios, ranging from 0.865 to 2.950, as compared to the average  $(^{230}\text{Th}/^{232}\text{Th})$  ratio of 1.002 in the cores.

For individual clast weathering transects,  $(^{238}\text{U}/^{232}\text{Th})$  and (230Th/232Th) ratios of the rind materials show three different groups of general patterns (Fig. 2; transects are marked in Fig. A1). Group 1 includes 6 weathering clasts that show general linear increases of both (238U/232Th) and (230Th/232Th) ratios with distance away from the core-rind boundary (AN-14-1.6, AN-14-19.6, AN-14-13.1, AN-14-13.2, AN-14-15.1, and AN-16-40.1; Fig. 2), similar to the patterns previously observed in weathering clasts from Ma et al. (2012), Engel et al. (2016), and Sak et al. (2018). In those studies, the linear increase was interpreted as the result of a continuous addition of uranium into the rind (relative to immobile Th) during rind formation; the excess <sup>234</sup>U in rind decays and produces <sup>230</sup>Th over time, leading to an increase of (<sup>230</sup>Th)<sup>232</sup>Th) ratios with distance into rind with time. Group 2 includes 2 samples, AN-14-40.2 and AN-14-19.4 that show elevated ( $^{238}$ U/ $^{232}$ Th) ratios near the core-rind boundary but the ratios remain constant in the rest of the rind (Fig. 2 and Fig. A2). The  $(^{230}\text{Th}/^{232}\text{Th})$  ratios show a continuous increase from the core into the rind. Such a pattern was first observed in a weathering clast from Costa Rica (Pelt et al., 2008) and was attributed to a process that added uranium instantaneously in the rind near the core-rind boundary, but the rest of the rind remained as a closed system with no further ura-

<sup>\*</sup> Clast samples from previous studies (Ma et al., 2012, 2018; Engel et al., 2016; Sak et al., 2018).

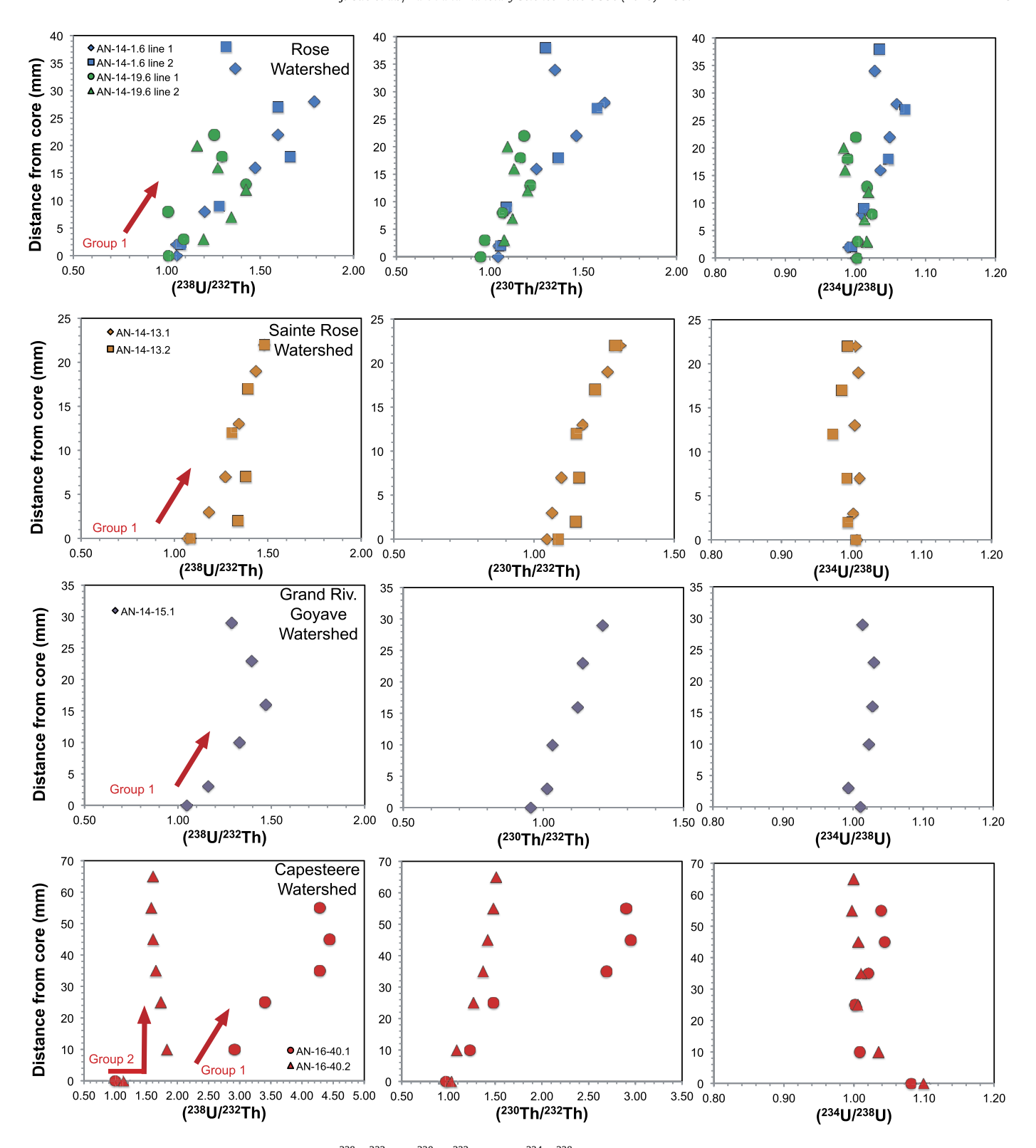


**Fig. 2.** Measured U-Th activity ratios in rind samples:  $(^{238}\text{U}/^{232}\text{Th})$ ,  $(^{230}\text{Th}/^{232}\text{Th})$ , and  $(^{234}\text{U}/^{238}\text{U})$  plotted as a function of position relative to the core-rind boundary (mm) along individual rind transects. Core samples plotted at position 0 mm. U-series analytical error bars are smaller than the symbol sizes. The locations of these 9 transects on individual clast samples are shown in clast images (Appendix Fig. A1). Clast samples are grouped into three categories based on their  $(^{238}\text{U}/^{232}\text{Th})$  patterns (see main text for details). Group 1: continuous U addition; Group 2: instantaneous U addition; and Group 3: no systematic patterns. Results from Group 3 clasts are shown in Appendix Fig. A2.

nium addition. Group 3 includes samples AN-14-3.5, AN-14-17.2 and AN-14-25.3 that do not show any systematic changes of  $(^{238}\text{U}/^{232}\text{Th})$  and  $(^{230}\text{Th}/^{232}\text{Th})$  ratios with distance (Fig. A2; Appendix 2). The U-series systematics in Group 3 clasts may have

experienced complicated condition changes of conditions in rind that could possibly lead to later loss of or further addition U. The mechanistic interpretations of the three different U-series patterns in clasts are further discussed in Section 5.2 below.

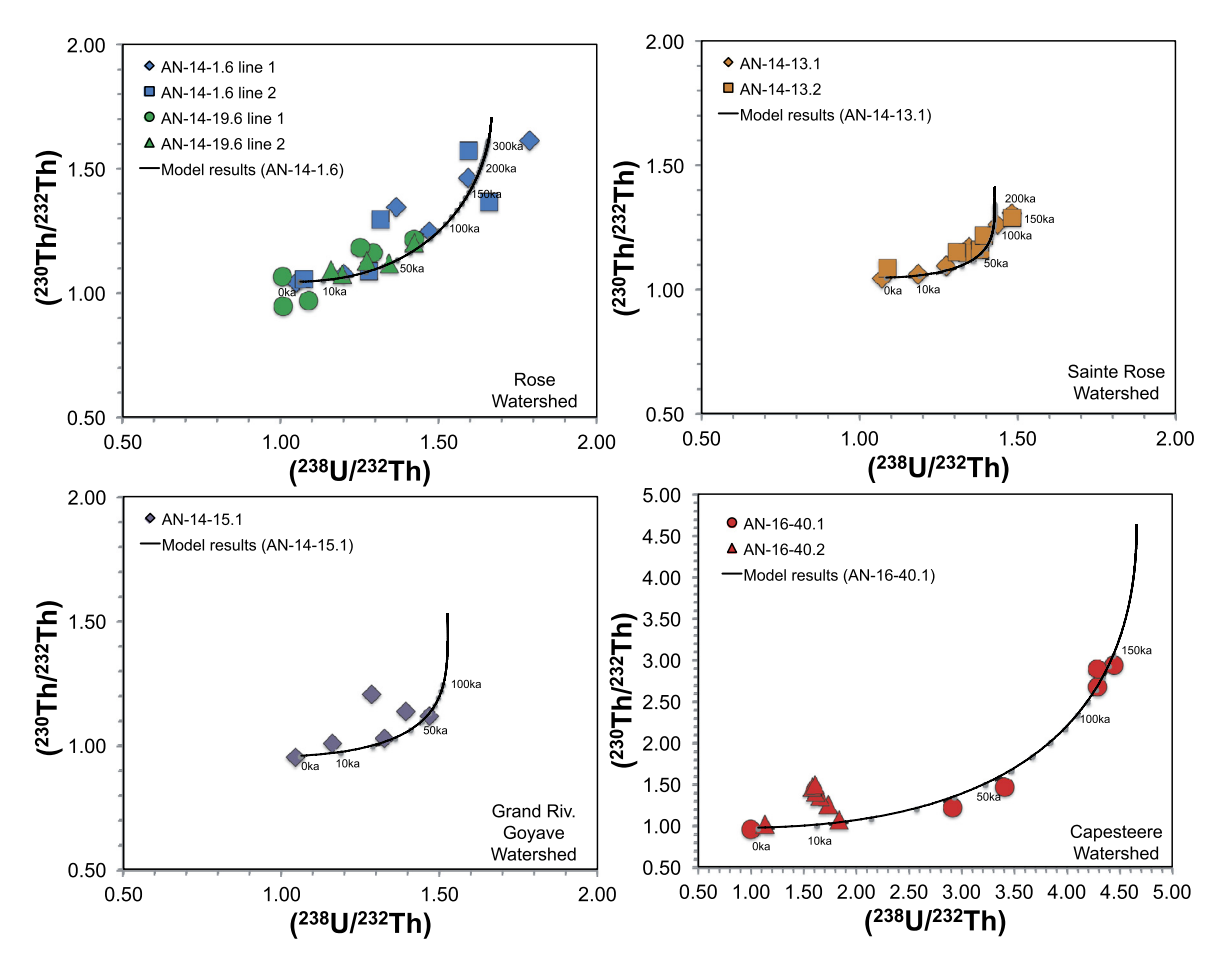


Fig. 3.  $(^{230}\text{Th})^{232}\text{Th})$  vs.  $(^{238}\text{U})^{232}\text{Th})$  isochron diagrams for weathering clasts of Basse-Terre Island in this study. The analytical error bars are within the symbol size. Core samples are at secular equilibrium (1.0). The U-Th radioactive disequilibria of the weathering rind samples from these 9 clast transects are best explained by (Group 1) continuous input of U plus leaching of U starting at the core-rind boundary (the modeled  $(^{238}\text{U})^{232}\text{Th})$  and  $(^{230}\text{Th})^{232}\text{Th})$  ratios with model parameters in Table 2 and their corresponding rind formation ages are shown as the black line with gray dots for selected transects from Group 1 clasts). Group 2 clast (AN-16-40.2) is best modeled by instantaneous input of U at the core-rind boundary without additional loss of U, and subsequent production of  $^{230}\text{Th}$  from U-series decay series in the rind (rind formation ages are shown in Table 2).

# 4.3. Determination of weathering advance rates in weathering clasts

The U-series disequilibrium generated during rind formation can be used to derive time information related to duration and intensity of chemical weathering (e.g., Chabaux et al., 2008; Dosseto et al., 2008). Recent successes of using U-series isotopes to quantify Earth surface processes have been highlighted by their applications in weathering clasts, soil profiles, sediments, and streams and rivers from small and large watersheds (Chabaux et al., 2008). In particular, the determination of weathering advance rates in weathering rinds relies on the use of U-series mass balance models that account for chemical leaching and addition of U-series isotopes during rind formation. Based on the general patterns observed in U-series profiles, two types of U-series mass balance models have been used (Dequincey et al., 2002; Pelt et al., 2008; Dosseto et al., 2008; Ma et al., 2012). The first type assumes a dual process of continuous U-series isotope leaching and addition in an open system (Dequincey et al., 2002), i.e., as the continuous U addition pattern observed in the Group 1 clasts above. The second type relies on an instantaneous addition of U-series isotopes during the initial stage of chemical weathering near the core-rind boundary, and the system remains closed after uranium addition (Pelt et al., 2008), as observed in the Group 2 clasts above. In this study, we follow the mobility behavior of U-series isotopes during rind formation and apply the continuous U addition model and the instantaneous addition model to Group 1 and Group 2 clasts, respectively, to calculate

rind ages and rind formation rates (Fig. 3; model calculations are presented in Appendix 3). Group 3 clasts cannot be used to calculate rind ages or rates due the lack of systematic U-series patterns (see Section 5.2 for further discussion). Of the 8 clasts used in model calculations, weathering transects from 7 clasts successfully yielded formation ages with the U-series mass balance models (Fig. 3) and clast AN-14-19.4 did not yield any formation ages (Appendix 3). The total rind formation ages for all rind transects vary from  $\sim$ 60 kyr to  $\sim$ 300 kyr (Table 2). Along these weathering rind transects, the rind ages generally increase with distance away from the core-rind boundary (Table 2; Fig. 4), and the average weathering advance rates range from 0.12 mm/kyr to 0.34 mm/kyr (Table 3). Model-derived k238U values from the six weathering clasts vary from  $1.5 \times 10^{-5}$  to  $4.8 \times 10^{-5}$  yr<sup>-1</sup> (Table 3), within the range of <sup>238</sup>U rate constants derived from weathering profiles or river sediments with similar weathering time scales (Dosseto et al., 2008; Ma et al., 2010; 2013; Engel et al., 2016). Similarly, model-derived k<sub>234</sub>/k<sub>238</sub> ratios are all greater than one, varying from 1.1 to 1.5 (Table 3), consistent with the fact that <sup>234</sup>U isotope is preferentially lost to the weathering fluids compared to <sup>238</sup>U (e.g., Fleischer, 1980). Such a range of values agrees well with many field and experimental studies of U isotopic fractionation during water-rock interaction (e.g., Vigier et al., 2001; Dequincey et al., 2002; Dosseto et al., 2008; Andersen et al., 2009). Model results also indicate that the rind experienced addition of U with f values ranging from 2.3  $\times$  10<sup>-5</sup> to 8.7  $\times$  10<sup>-5</sup> yr<sup>-1</sup>. The f

**Table 2**Rind formation ages and model parameters

Clast name	Sample name	Distance from core (mm)	Weathering age (ky)	+/- (1SD, ky)	Model parameters	Median value	+/- (1SD)
AN-16-1.6	1.6 Core	0			f <sup>238</sup> U	2.31E-05	9.09E-06
10 110	1.6 Ba	2	2	3	f <sup>234</sup> U/f <sup>238</sup> U	1.24E+00	1.60E-01
	1.6 Bb	8	19	11	k <sup>238</sup> U	1.46E-05	5.96E-06
	1.6 Bc	16	80	28	k <sup>234</sup> U/k <sup>238</sup> U	1.21E+00	1.70E-01
	1.6 Bd	22	165	33	Goodness of fit (Chi <sup>2</sup> )	1.52E+01	1.50E+00
	1.6 Be	28	300	66	Goodiless of the (CIII )	1.52L+01	1.50L+00
	1.6 Bf	34	300	00			
	1.6 Ta	2	3	3			
		9	31				
	1.6 Tb 1.6 Tc	18	142	14 37			
	1.6 Td	27	218	33			
	1.6 Te	38	210	33			
AN-14-19.6	19.6 Core	0			f <sup>238</sup> U	5.51E-05	2.21E-05
	19.6 a3	3	7	6	$f^{234}U/f^{238}U$	1.27E+00	1.64E-01
	19.6 b1	8	2	3	k <sup>238</sup> U	3.89E-05	1.59E-05
	19.6 c1	13	112	22	$k^{234}U/k^{238}U$	1.27E+00	1.77E-01
	19.6 d1	18			Goodness of fit (Chi <sup>2</sup> )	6.39E+00	2.94E-01
	19.6 e1	22			, ,		
	19.6 p1	3	27	15	f <sup>238</sup> U	5.50E-05	2.47E-05
	19.6 q1	7	70	18	f <sup>234</sup> U/f <sup>238</sup> U	1.45E+00	2.40E-01
	19.6 r1	12	116	21	k <sup>238</sup> U	3.98E-05	1.83E-05
		16	110	21	k <sup>234</sup> U/k <sup>238</sup> U	1.46E+00	2.52E-01
	19.6 s1 19.6 t1	20			Goodness of fit (Chi <sup>2</sup> )	4.77E+00	2.32E-01 1.47E+00
AN-14-13.1	13.1 Core	0			f <sup>238</sup> U	5.50E-05	2.77E-05
	13.1 a	3	14	11	f <sup>234</sup> U/f <sup>238</sup> U	1.35E+00	2.27E-01
	13.1 b	7	30	20	k <sup>238</sup> Ú	4.12E-05	2.11E-05
	13.1 c	13	61	27	$k^{234}U/k^{238}U$	1.37E+00	2.41E-01
	13.1 d	19	128	34	Goodness of fit (Chi <sup>2</sup> )	4.08E+00	1.34E+00
	13.1 e	22	179	50	, , ,		
AN-14-13.2	13.2 Core	0			f <sup>238</sup> U	6.34E-05	2.52E-05
	13.2e	2	52	17	f <sup>234</sup> U/f <sup>238</sup> U	1.46E + 00	2.66E-01
	13.2f	7	66	18	k <sup>238</sup> U	4.84E-05	1.97E-05
	13.2g	12	45	16	$k^{234}U/k^{238}U$	1.51E+00	2.77E-01
	13.2h	17	101	21	Goodness of fit (Chi <sup>2</sup> )	5.69E + 00	1.57E+00
	13.2i	22	184	34			
AN-14-15.1	15.1 Core	0			f <sup>238</sup> U	5.21E-05	2.57E-05
	15.1 a1	3	10	4	$f^{234}U/f^{238}U$	1.18E+00	1.14E-01
	15.1 b1	10	28	8	k <sup>238</sup> U	3.57E-05	1.92E-05
	15.1 c1	16	60	8	$k^{234}U/k^{238}U$	1.18E+00	1.45E-01
	15.1 d3 15.1 e1	23 29			Goodness of fit (Chi <sup>2</sup> )	1.66E+00	5.16E-01
AN-16-40.1	40.1 Core	0			f <sup>238</sup> U	8.71E-05	1.72E-05
, 10 10,1	40.1 0-2 cm	10	40	9	f <sup>234</sup> U/f <sup>238</sup> U	1.02E+00	1.84E-02
	40.1 0-2 cm				k <sup>238</sup> U		
		25	56	11	k <sup>234</sup> U/k <sup>238</sup> U	1.87E-05	4.31E-06
	40.1 3-4 cm	35	124	14		1.03E+00	4.17E-02
	40.1 4-5 cm 40.1 5-6 cm	45 55	144 137	14 14	Goodness of fit (Chi <sup>2</sup> )	2.19E+01	2.19E+01
AN-16-40.2	40.2 Core	0					
	40.2 0-2 cm	10	8				
	40.2 2-3 cm	25	45				
	40.2 3-4 cm	35	82				
	40.2 4-5 cm	45	115				
	40.2 5-6 cm	55	191				
	40.2 6-7 cm	65	192				

values are all greater than the k values for the six weathering clasts (Table 3), indicating net addition of U to the rind due to the dual processes of U mobility. The model derived  $f_{234}/f_{238}$  ratios are also greater than one (1.02 to 1.46), consistent with U addition from the infiltrating soil water that is generally characterized by ( $^{234}U/^{238}U$ ) > 1. For each profile, the derived  $f_{234}/f_{238}$  value is similar to the derived  $k_{234}/k_{238}$  value, implying that the dual processes of U mobility could lead to either increases of ( $^{234}U/^{238}U$ ) ( $f_{234}/f_{238}$  >  $k_{234}/k_{238}$ ) or decrease of ( $^{234}U/^{238}U$ ) ( $f_{234}/f_{238}$  <  $k_{234}/k_{238}$ ) with

time (Dequincey et al., 2002), consistent with the observed non-linear changes of  $(^{234}U/^{238}U)$  ratios in the rinds (Fig. 2).

# 5. Discussion

# 5.1. Mobility behavior of U-series isotopes during rind formation

Uranium is soluble and highly mobile during water-rock interactions under oxidizing conditions. The minor isotope of U,  $^{234}$ U, is preferentially released to solution compared to  $^{238}$ U, due to the alpha recoil effect of  $^{238}$ U decay that either ejects  $^{234}$ U particles

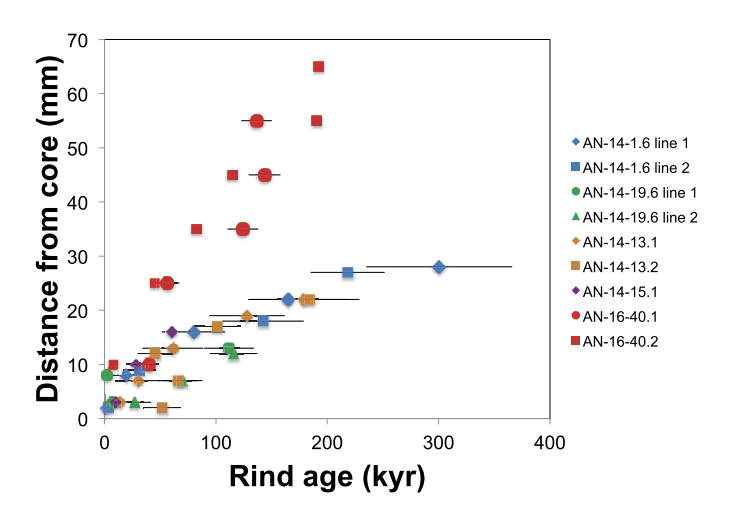


**Fig. 4.** Rind formation age vs. distance relative to the core–rind boundary for the 9 rind transects in this study. Slope of each linear trend represents the weathering advance rate of the core–rind boundary (or rind weathering rate) for each transect (the slope values or the rates and  $R^2$  values are provided in Table 3). Regressions were forced through the origin as we define position 0 (core–rind boundary) as the start point (t=0) for chemical weathering.

Table 3
Weathering advance rates from weathering clasts of Basse-Terre Island.

Clast	Weathering rate	$R^2$
name	(mm/kyr)	
AN-14-1.6 line 1	0.109	0.70
AN-14-1.6 line 2	0.127	0.92
AN-14-19.6 line 1	0.119	0.29
AN-14-19.6 line 2	0.108	0.99
Average rate	$0.116 \pm 0.008$	
AN-14-13.1	0.139	0.85
AN-14-13.2	0.129	0.67
Average rate	$0.134 \pm 0.007$	
AN-14-15.1	$0.282 \pm 0.010$	0.94
AN-16-40.1	0.338	0.85
AN-16-40.2	0.338	0.84
Average rate	$0.338 \pm 0.010$	
AN-14-3 <sup>a</sup>	$0.22 \pm 0.15$	0.89
AN-14-6 <sup>b</sup>	$0.18 \pm 0.07$	0.87
AN-14-7 <sup>€</sup>	$0.08\pm0.04$	0.75

- <sup>a</sup> From Sak et al. (2018); Ma et al. (2018).
- b From Ma et al. (2012).
- <sup>c</sup> From Engel et al. (2016).

directly to fluids, or damages the crystal lattice and releases 234U easily during subsequent weathering (e.g., Fleischer, 1980). Water phases are thus characterized by  $(^{234}U)^{238}U)$  activity ratios > 1 while solid residual weathering products with (234U/238U) activity ratios < 1 (e.g., Rosholt et al., 1966; Vigier et al., 2001; Chabaux et al., 2003, 2008; Dosseto et al., 2008; Anderssen et al., 2009). However, the rind  $(^{234}U)^{238}U$ ) values in this study, as in solid residual weathering products, show disequilibrium signatures both below and above one (0.964 to 1.071; Table A2). Such an observation reveals a dual process of U mobility during rind formation: (1) chemical leaching that generates  $(^{234}U/^{238}U)$  ratios < 1 in the rind; and (2) addition of U with  $(^{234}U)^{238}U$ ) ratios > 1, such as precipitate or sorbate to the rind from infiltrating soil pore water that generally carries ( $^{234}U/^{238}U$ ) ratios > 1. The dual processes of U mobility during weathering could lead to either increases of  $(^{234}\text{U}/^{238}\text{U})$  or decrease of  $(^{234}\text{U}/^{238}\text{U})$  in rinds with time, depending on the relative intensity of these two processes.

Rind  $(^{238}\text{U}/^{232}\text{Th})$  activity ratios of these clasts are higher than the average core  $(^{238}\text{U}/^{232}\text{Th})$  ratios (Fig. 2). The elevated  $(^{238}\text{U}/^{232}\text{Th})$  activity ratios show evidence of U addition (or U im-

mobilization) during rind formation, as thorium is generally immobile during water-rock interaction due to its extremely low solubility in water (e.g., Rosholt et al., 1966; Chabaux et al., 2003). The assumption of Th immobility in weathering rinds has been justified by comparing Th profiles with other immobile elements such as Ti and Zr (e.g., Ma et al., 2012, 2018; Engel et al., 2016; Ma, 2018). U immobilization could occur when the environmental conditions change from oxidizing to reducing conditions, under which the solubility of U-containing phases is much lower (Chabaux et al., 2003, 2008 and references therein), or due to co-precipitation or sorption of U onto newly formed secondary minerals such as Fe-hydroxides (Ames et al., 1983; Duff et al., 2002; Chabaux et al., 2003, 2008 and references therein). In a weathering clast system, the rind material is generally dominated with highly oxidized minerals, e.g. Fe oxy-hydroxides, and the unweathered core contains reduced minerals such as pyroxene and ilmenite. It is possible that the rind-core boundary marks a redox transition zone with oxidizing conditions in outer rinds to reducing conditions near the core-rind boundary. The reducing conditions in the innermost rind could lead to the first precipitation of the dissolved U from infiltration soil pore water. The fate of this added U could depend on later processes in the rind, possibly controlled by the mineralogy transformation of Fe oxy-hydroxides. For example, it has been shown that newly formed secondary Fe-hydroxides have large and highly reactive surface areas (e.g., Pett-Ridge et al., 2007) that could promote further co-precipitation or sorption of U from soil water to rind. Such a process is consistent with the observation that the (238U/232Th) ratio increases continuously with distance away from the core-rind boundary (e.g., in Group 1 clasts, Fig. 2). If the U addition to the rind were more sensitive to the redox conditions at the core-rind boundary than the adsorption onto Fe-hydroxides, then no subsequent addition of U would occur in the rind. This would lead to an instantaneous U addition profile in rinds (e.g., in Group 2 clasts, Fig. 2). Any further changes of conditions in rind could also possibly lead to later loss or addition of U in the rind that could lead to complicated U profiles (such as in Group 3 clasts). Indeed, the affinity of U to Fe-hydroxides is sensitive to their morphology and crystalline states. U is strongly associated with amorphous and poorly crystalline Fe-oxides. Any later transformation into more organized and crystalline Fe-oxides could lead to a weak association with U (or other particle reactive elements such as P) or U loss (Pett-Ridge et al., 2007; Thompson et al., 2011; Hall and Silver, 2015). Group 3 clasts could be affected by this modification process and show no systematic U-series patterns (Fig. A2). Some of the outmost rinds in Group 1 clasts also show possible evidence of U loss (Fig. 2). To summarize, redox conditions and mineralogy and morphology states of the Fe-oxides in rinds play an important role in controlling U mobility history and generate the possible three different patterns of U profiles in these rinds, with significant implications on how to use U-series isotopes to determine rind formation ages and rates (Appendix 2).

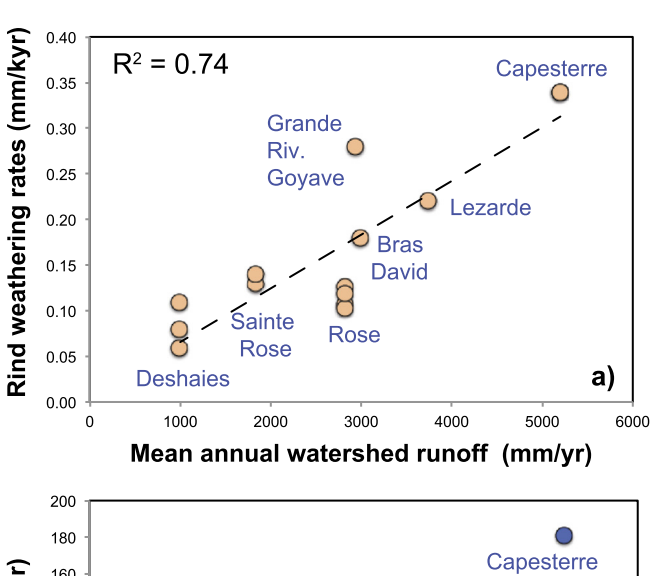
# 5.2. Long-term chemical weathering rates on Basse-Terre Island

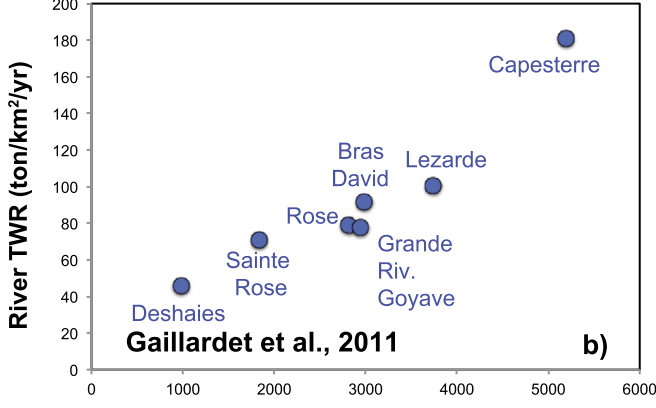
Rind formation rates, or weathering advance rates (the rate at which the core-rind boundary migrates into the core) were calculated based on the observed U-series disequilibria, following the continuous U addition model or the instantaneous U addition model (Fig. 4). In combination with three previous studies (Ma et al., 2012; Engel et al., 2016; Sak et al., 2018), weathering advance rates in seven watersheds (in one watershed the clast rates were not available) on Basse-Terre Island are compiled from a large number of weathering clasts for the first time (Table 3). The seven watersheds of the island are characterized with strong environmental gradients (Table 1; Fig. 1). For example, the water-

shed relief decreases from southeast to northwest, and the mean annual precipitation (MAP) and watershed runoff values also decrease systematically from southeast to northwest. The mean annual air temperatures (MAT) of the clast sampling sites in these watersheds have a limited range (23 to 25 °C).

The rind advance rates in these watersheds range from 0.08 to 0.34 mm kyr<sup>-1</sup>, with values increasing systematically from northwest to southeast (Table 3). These rates were all determined from the rind transects perpendicular to the core-rind boundary with low curvature values (e.g., flat core-rind boundaries), hence by similar curvature control of core-rind boundary (Sak et al., 2010; Ma et al., 2012; Lebedeva et al., 2015). The rind weathering rates do not appear to correlate with the clast scale parameters such as total rind thickness, clast size, or shape (Table A1), but show a strong and positive correlation with the water availability parameters at the watershed scale, such as the mean runoff values and MAP for individual watersheds (Fig. 5). The reported annual runoff values for the individual watersheds are constrained by  $\sim 10$ years of field measurements and monitoring programs for the main rivers on Basse-Terre Island (Gaillardet et al., 2011) and show the most significant correlation ( $R^2 = 0.74$ ) with rind weathering rates (Fig. 5). Relatively weak but still significant and positive correlations were observed between MAP and rind weathering rates  $(R^2 = 0.30 \text{ to } < 0.10, \text{ depending on the MAP data sources; Fig. A3}).$ 

In a weathering clast, the weathering advance rate is determined not only by curvature, initial mineralogical content, and solute transport characteristics, but also by solute concentrations (i.e., C in weathering fluids such as infiltrating soil water) (e.g., Eqn. (30) in Lebedeva et al., 2015). For example, the advance rate (W) should be a direct function of  $(C^e - C^R)$ :  $C^e$  is the equilibrium concentration at the temperature of interest, and  $C^R$  is the concentration of this component in the pore fluid at the outermost boundary of the weathering clast, e.g., in infiltrating soil water. Weathering at the same temperature but under higher rates of precipitation and infiltration are expected to have more dilute soil water and therefore higher values of  $(C^e - C^R)$ . If  $(C^e - C^R)$  varies linearly with annual watershed runoff or MAP, then the Lebedeva et al. (2015) model is consistent with the observed positive linear correlation between weathering advance rates and annual watershed runoff values (Fig. 5). Remarkably, this observation not only confirms the observation of modern river chemical fluxes at Basse-Terre Island, but also highlights the important control of orographic precipitation on chemical weathering at a geological time scale for Basse-Terre Island. Indeed, river chemistry data of Basse-Terre Island has shown a strong correlation between a catchmentwide chemical weathering rate (46 to 181 t/km<sup>2</sup>/yr) and the annual watershed runoff (1000 to 5200 mm/yr) for the studied seven watersheds (Table 1; Gaillardet et al., 2011). As mentioned above, at a watershed scale, for an increase in runoff, hydrological buffering mechanisms maintain the concentration of solutes despite the effect of dilution, leading to the observed correlation between riverine weathering fluxes and annual watershed runoff (i.e. "the chemostastic effect"; e.g. Godsey et al., 2009; Gislason et al., 2009; Maher, 2010). The rind weathering advance rates were determined at a time scale of tens to hundreds of thousands years, i.e. the rates were averaged over the total weathering duration of the rinds between 60 to 300 kyrs (Table 2), much longer than the contemporary chemical weathering fluxes measured in river chemistry. The weathering advance rates were also determined in rinds independently without relying on any existing river runoff values in the calculations. Hence, the correlation between weathering rates and watershed runoff values does not involve the same mathematical complication as the calculations of the riverine weathering fluxes. This weathering rind-based approach confirms the important observations from the riverine studies by providing independent and long term weathering rates.





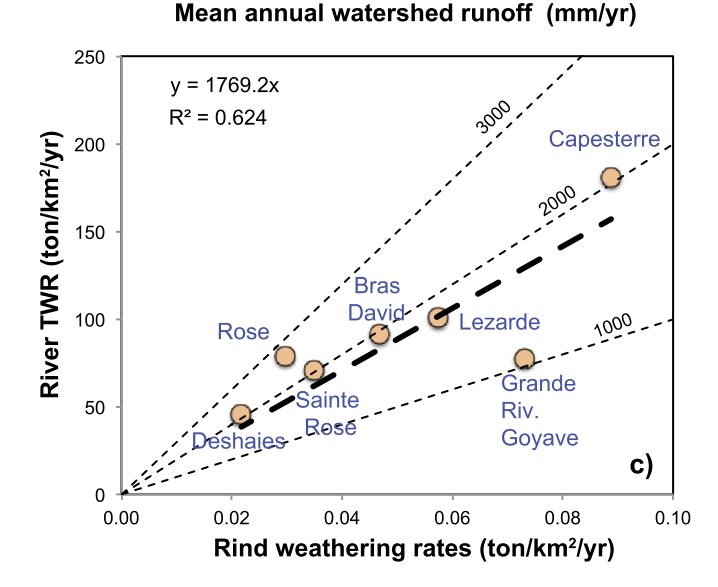


**Fig. 5. a)** Rind weathering rates (mm/kyr) plotted as a function of mean annual watershed runoff (mm/yr) for weathering clasts from Basse-Terre. The watershed runoff values are from Gaillardet et al. (2011). The dash line indicates a linear fit between these two variables ( $R^2 = 0.74$ ). Rind weathering rates also show positive correlation with MAP (Appendix Fig. A3). **b)** River total weathering rates (TWR,  $ton/km^2/yr$ ) plotted as a function of mean annual watershed runoff (mm/yr) for the same watersheds of clast samples from Basse-Terre (Gaillardet et al., 2011). TWR were derived from river chemistry and annual runoff for each watershed on Basse-Terre Island and represent weathering rates at the watershed scale (Gaillardet et al., 2011). **c)** Rind weathering rates (converted to  $ton/km^2/yr$  at the clast scale, values of multiple clasts from each watershed were averaged) vs. TWR (Total weathering rates for watershed,  $ton/km^2/yr$ ). Dashed line indicates the rate difference of these two sets of rates.

# 5.3. Reconciling difference in weathering rates between clast and watershed scales

The study of U-series systematics in weathering rinds expands our field toolbox for studying chemical weathering rates across scales. The weathering advance rates in rinds were reported as rock to rind conversion rate mm (rock)/kyr, or the volumetric rock to rind conversion rate, mm<sup>3</sup> (rock)/mm<sup>2</sup> (surface area)/kyr. Here the surface area refers to the geometric area on the clast that is perpendicular to the weathering advance direction. With a parent rock density of 2600 kg/m3 and the mass fraction of total cations (Na + K + Mg + Ca) in unweathered andesitic rock of 0.1 (Ma et al., 2012), the weathering advance rates of 0.08 to 0.34 mm<sup>3</sup>/mm<sup>2</sup>/kyr in this study correspond to 0.022 to 0.089 tons/km<sup>2</sup>(clast area)/yr for the loss of total cations during andesite weathering at the clast scale. These rind rates are three orders of magnitude slower (by  $\sim$ 1000 to 3000 times) than the river weathering fluxes derived from the corresponding individual watersheds (46 to 181 tons/km<sup>2</sup>/yr; Fig. 5). The rate discrepancy (clast vs. watershed) does not appear to vary with watershed characteristics from all the watersheds such as annual watershed runoff, relief, bedrock age, or watershed size (Fig. A4), but remains relatively constant, with an average of  $\sim$ 1800  $\pm$  400 times.

Such a comparison is consistent with the previous observations that chemical weathering rates generally do not agree across scales and can differ by orders of magnitude. The discrepancy has been attributed to differences in measurements of weathering rates such as duration of weathering (White and Brantley, 2003; Maher et al., 2004), hydrologic regime and flow path factors (Velbel, 1993; Pacheco and Alencoao, 2006), factors related to clay precipitation (Maher, 2010), and methods used to measure surface area or the presence of surface coatings (Nugent et al., 1998; Maher et al., 2006; Navarre-Sitchler and Brantley, 2007), the influence of biota or organic acids (Wasklewicz, 1994; Drever and Stillings, 1997), ongoing removal of weathered materials by physical erosion (i.e., Bluth and Kump, 1994; Dupre et al., 2003; Anderson, 2005; West et al., 2005), and a scale effect of time-dependent mineral dissolution (Jung and Navarre-Sitchler, 2018). In this study, the weathering clasts were collected from the watersheds where the river weathering fluxes were measured with the same climate conditions (mean air temperature, precipitation, and river runoff) and general topographic features (average relief). The weathering materials in the two different systems of this study, i.e. the core materials of the weathering clasts and the bedrock materials in watersheds, have similar chemical and mineralogy compositions as observed from local outcrops and quarries (Sak et al., 2010: Ma, 2018). One possible exception is that weathering materials in watersheds could include porous and more readily weathered pyroclastic flows. However, the contribution from weathering of pyroclastic flows may not be constant across individual watersheds and hence cannot explain the relatively constant difference in weathering rates reported in the two weathering systems (clast vs. watershed). The rate difference thus cannot be attributed to different field conditions or parent materials.

In this study, we follow the notation that the surface areas for weathering clasts *vs.* watershed are measured and reported by using different "rulers" at different spatial scales (Navarre-Sitchler and Brantley, 2007). The rind rates were measured at the weathering interface of core-rind boundary with a length scale at the level of mm while the river weathering fluxes were measured in rivers that collect weathering products from watersheds at the length scale of km. To reconcile the rate discrepancy, Navarre-Sitchler and Brantley (2007) proposed that the rate of weathering of basalt was constant when compared across scales, from the laboratory to clasts to soil profiles to watersheds, only when normalized by

the "real" basalt surface area that actually experienced weathering ( $A_{weathering}$ ). However, because the value of  $A_{weathering}$  is not known at each scale, the weathering rate was instead reported as a rate normalized by the surface area assessed at that spatial scale ( $A_{measured}$ ), not the actual  $A_{weathering}$ . For example, the geographic area of a watershed  $(A_{watershed})$  is not comparable in magnitude with the surface area estimated from the geometry of a clast  $(A_{clast})$ , but they are fractal in that they vary with the scale of measurement. In addition, Navarre-Sitchler and Brantley (2007) pointed out that the surface area of a weathering front varies by two types of fractal dimension,  $d_r$  and  $d_s$ . The  $d_r$  value represents the undulation of the surface area and the  $d_s$  value represents the presence of more particles within the thickness of the reaction front. For a simple comparison, Navarre-Sitchler and Brantley (2007) introduced the ratio of  $A_{weathering}/A_{watershed}$ , or,  $A_{weathering}/A_{clast}$  as the roughness ( $\lambda$ ) value at the watershed or clast scale. With this approach, the basalt weathering rates compiled from a global dataset across scales were predicted with the equation (Navarre-Sitchler and Brantley, 2007):

$$W_D^{\beta} = k_0 \left(\frac{\beta}{a}\right)^{d_r - 2} e^{-E_a/RT} \tag{6}$$

Here  $W_D$  is the weathering rate (mm³ mm $^{-2}$  yr $^{-1}$ ) measured at the scale of lab-BET, lab-geometry, clast, soil, or watershed, respectively;  $\beta$  indicates the length scale (mm) for each scale;  $k_0$  is the pre-exponential factor,  $E_a$  is the activation energy, a is a spatial constant related to the BET length scale ( $a=10^{-7}$  mm), R is gas constant and T is the temperature;  $d_r$  is the fractal dimension that relates surface areas across scales (e.g.,  $d_r \sim 2.3$  for basalt weathering; Navarre-Sitchler and Brantley, 2007); and  $(\frac{\beta}{a})^{d_r-2}$  is the roughness term ( $\lambda$ ). If we focus on comparing the rate difference across scales for Basse-Terre Island, Equation (6) can be rearranged to highlight the rate difference across scales:

$$\frac{W_D^{\beta}}{(\frac{\beta}{a})^{d_r-2}} = k_0 e^{-\frac{E_a}{RT}} = constant,$$

$$\frac{W_{BET}^{\beta}}{(\frac{\beta_{BET}}{a})^{d_r-2}} = \frac{W_{GEO}^{\beta}}{(\frac{\beta_{GEO}}{a})^{d_r-2}} = \frac{W_{Clast}^{\beta}}{(\frac{\beta_{Clast}}{a})^{d_r-2}} = \frac{W_{Soil}^{\beta}}{(\frac{\beta_{Soil}}{a})^{d_r-2}}$$

$$= \frac{W_{Watershed}^{\beta}}{(\frac{\beta_{Watershed}}{a})^{d_r-2}} \tag{7}$$

here  $\beta$  is assumed to be  $10^{-7}$  mm (BET),  $10^{-3}$  mm (GEO), 1 mm (clast), 10 mm (or 1 cm, soil), and  $10^6$  mm (or 1 km, watershed); and a is  $10^{-7}$  mm (BET) as defined by Navarre-Sitchler and Brantley (2007).

If we assume that the rate difference observed between the clast and the watershed scale  $(W_{Watershed}/W_{Clast} = 1800 \pm 400)$ is attributed to the fractal control on the roughness difference across scales, then the fractal dimension  $d_r$  is  $\sim 2.54 \pm 0.02$  for andesite weathering at Basse-Terre by solving Eqn. (7) (Fig. 6). This value is similar to the  $d_r$  value for the global basalt weathering study (2.3; Navarre-Sitchler and Brantley, 2007). The  $d_r$  value (>2) represents the undulations in the bedrock-saprolite contact, or the deep weathering front that is not easily accessible at the watershed scale. The weathering front roughness for the weathering clast is visible from the sectioned weathering clasts (e.g., Fig. A1) while it is hard to measure the roughness for the bedrocksaprolite contact in a watershed. It can be reasonably assumed that the bedrock-saprolite contact at the watershed scale has more pronounced undulation features than the core-rind boundary at the clast scale. Hence, the surface area available for weathering at

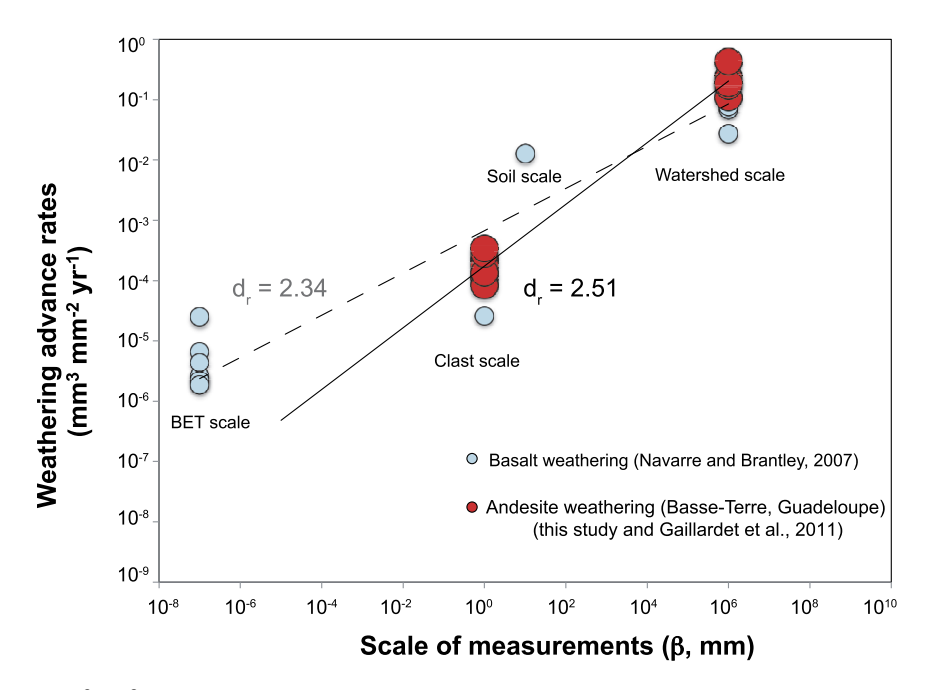


**Fig. 6.** Weathering advance rates (mm<sup>3</sup>/mm<sup>2</sup>/yr) for Basse-Terre Island plotted as a function of the scale length at which the surface area is assessed (β, mm; watersheds are assumed with 1 km, or 10<sup>6</sup> mm length scale and clasts are assumed with 1 mm length scale). Figure shows that advance rates vary with the length scale and can be reconciled with Equation (7), following the fractal dimension factor  $d_T = 2.51$ . Clast scale rates are from this study and watershed scale rates are from Gaillardet et al. (2011). Basalt weathering rates across scales from Navarre-Sitchler and Brantley (2007) are shown for comparison.

the bedrock-saprolite contact is larger than the core-rind boundary, with a higher weathering rate controlled by the increase of scale length in the fractional dimension (Eqn. (7)). The increase of weathering rates across scales could also be due to the increase of particle numbers available for weathering to occur within the weathering front (e.g., at the fractal scale, the fractal dimension is controlled by the factor  $d_s$ ). For example, widely spaced fracture systems are known to exist at the bedrock-saprolite contact at watershed scales and could supply additional particles (and surfaces) for weathering to occur, as compared to the weathering clast system in which the core-rind boundary is sharp and with no visible networks of fractures in cores. Hence, following the interpretation of Navarre-Sitchler and Brantley (2007), the presence of the undulations and fractures (e.g. roughness with fractal dimensions) at the bedrock-saprolite contact at the watershed scale is most likely the main factor contributing to the  $\sim$ 1800 times apparent faster weathering rates observed at the watershed scale relative to that observed at the clast scale.

Other processes could also contribute to the different weathering rates observed between the watershed and the clast scales for the volcanic island of Basse-Terre, such as weathering of pyroclastic flows and ash layers, impacts of hydrothermal sources, different regolith thickness with deep vs. shallow weathering fronts, and shallow vs. deep groundwater flow paths. However, most of the above processes cannot offer a reasonable controlling mechanism that leads to a relative constant difference between the two sets of weathering rates. The rate difference is best reconciled by using the fractal dimension in surface roughness across scales.

# 6. Conclusions

Our study systematically investigated U-series disequilibria and derived rind formation ages and weathering rates in a large number of weathering clasts collected from eight watersheds on Basse-Terre Island. Total rind formation ages in these rinds range from 60 kyr to 300 kyr, indicating these weathering clasts formed from andesitic rock fragments or volcanic clasts in soil zones over long time scales. For each individual transect, the rind ages generally

increase with distance away from the core-rind boundary. The weathering advance rates from these rinds range from 0.08 to  $0.34 \text{ mm kyr}^{-1}$ , with a strong positive correlation with the watershed annual runoff values, confirming the previous observation in riverine studies, but now determined independently. Both the rind weathering rates and river weathering fluxes show similar positive correlation with annual watershed runoff values, suggesting that the control of water cycle on chemical weathering operates similarly at both short- and long-time scales for tropical volcanic Basse-Terre Island. Furthermore, these rind weathering rates are slower than the river weathering fluxes derived from the corresponding individual watersheds, by a constant difference of  $\sim$ 1800  $\pm$  400 times despite changes in watershed characteristics. We reconcile the rate difference at Basse-Terre Island by attributing to the fractal dimension control on the roughness and surface area across scales (Navarre-Sitchler and Brantley, 2007). The presence of undulations and fractures (e.g. roughness) at the bedrock-saprolite contact at the watershed scale is not assessed at the watershed scale and is most likely the main fractal dimension control that contribute to  $\sim$ 1800 times rate discrepancy observed between the watershed scale and the clast scale. U-series isotope systematics in weathering rinds provides a new useful tool to quantify how weathering interface advances in weathering clasts and to reconcile rates from difference spatial scales.

# Acknowledgements

We would like to thank two anomynous reviewers for their insightful comments that improved the original manuscript and Editor-in-Chief Dr. Itay Halevy for his effective editorial handling of the submissions. This research was funded by the National Science Foundation grants EAR1251952, EAR1251969, and EAR1251875. We thank the Parc National de Guadeloupe for authorizing us sampling in the National Park. We thank Celine Dessert (IPGP) and L'Observatoire Volcanologique et Sismologique de Guadeloupe (IPGP) and the Critical Zone Observatory ObErA (PI. E. Lajeunesse) for providing logistical support. Jieye Guo thank CZO SAVI Summer Interns Program for a scholarship to visit IPGP. LM also acknowl-

edged Dr. Mark Engle (USGS) for support on statistical analysis and Monte Carlo simulations. Insightful and fruitful discussion with S. Brantley at Penn State University, J. Bouchez and E. Lajeunesse at IPGP are appreciated.

### Appendix A. Supplementary material

Supplementary material related to this article can be found online at https://doi.org/10.1016/j.epsl.2019.115874.

#### References

- Allemand, P., Delacourt, C., Lajeunesse, E., Devauchelle, O., Beauducel, F., 2014. Erosive effects of the storm Helena (1963) on Basse Terre Island (Guadeloupe Lesser Antilles Arc). Geomorphology 206, 79–86.
- Ames, L.L., McGarrah, J.E., Walker, B.A., 1983. Sorption of trace constituents from aqueous solutions onto secondary minerals. I. Uranium. Clays Clay Miner. 31, 321–334.
- Andersen, M.B., Erel, Y., Bourdon, B., 2009. Experimental evidence for <sup>234</sup>U-<sup>238</sup>U fractionation during granite weathering with implications for <sup>234</sup>U/<sup>238</sup>U in natural waters. Geochim. Cosmochim. Acta 73, 4124–4141.
- Anderson, S.P., 2005. Glaciers show direct linkage between erosion rate and chemical weathering fluxes. Geomorphology 67, 147–157.
- Berner, R.A., Lasaga, A., Garrels, R.M., 1983. The carbonate-silicate geochemical cycle and its effect on atmospheric carbon dioxide over the past 100 million years. Am. J. Sci. 283, 641–683.
- Bluth, G.J.S., Kump, L.R., 1994. Lithologic and climatologic controls of river chemistry. Geochim. Cosmochim. Acta 58, 2341–2359.
- Bourdon, B., Bureau, S., Andersen, M.B., Pili, E., Hubert, A., 2009. Weathering rates from top to bottom in a carbonate environment. Chem. Geol. 258, 275–287.
- Bourdon, B., Henderson, G.M., Lundstrom, C.C., Turner, S.P., 2003. Uranium-series geochemistry. Mineral. Soc. Am. Rev. Mineral. Geochem. 52, 656.
- Brantley, S., Kubicki, J., White, A., 2008. Kinetics of Water-Rock Interaction. Springer. Brantley, S.L., White, T.S., White, A.F., Sparks, D., Richter, D., Pregizer, K., Derry, L., Chorover, J., Chadwick, O., April, R., Anderson, S., Amundson, R., 2006. Frontiers in Exploration of the Critical Zone: Report of a Workshop Sponsored by the National Science Foundation (NSF), October 24-26, 2005, Newark, DE, 30 p.
- Cernohouz, J., Solc, I., 1966. Use of sandstone wanes and weathered basaltic crust in absolute chronology. Nature 212, 806–807.
- Chabaux, F., Bourdon, B., Riotte, J., 2008. U-series geochemistry in weathering profiles, river waters and lakes. Radioact. Environ. 13, 49–104.
- Chabaux, F., Riotte, J., Dequincey, O., 2003. U-Th-Ra fractionation during weathering and river transport. Rev. Mineral. Geochem. 52, 533–576.
- Chatanantavet, P., Lajeunesse, E., Malverti, L., Meunier, P., Parker, G., 2010. Physically-based model of downstream fining in bedrock streams with side input. Water Resour. Res. 46, W02518. https://doi.org/10.1029/2008WR007208.
- Colman, S.M., Pierce, K.L., 1981. Weathering rinds on andesitic and basaltic stones as a Quaternary age indicator, Western United States. U.S. Geological Survey Professional Paper. 41 p.
- DePaolo, D.J., Maher, K., Christensen, J.N., McManus, J., 2006. Sediment transport time measured with U-series isotopes: results from ODP North Atlantic drift site 984. Earth Planet. Sci. Lett. 248, 394–410.
- Dequincey, O., Chabaux, F., Clauer, N., Sigmarsson, O., Liewig, N., Leprun, J.-C., 2002. Chemical mobilizations in laterites: evidence from trace elements and 238U-234U-230Th disequilibria. Geochim. Cosmochim. Acta 66, 1197–1210.
- Dessert, C., Lajeunesse, E., Lloret, E., Clergue, C., Crispi, O., Gorge, C., Quidelleur, X., 2015. Controls on chemical weathering on a mountainous volcanic tropical island: Guadeloupe (French West Indies). Geochim. Cosmochim. Acta 171, 216–237
- Dessert, C., Dupré, B., Gaillardet, J., Francois, L., Allègre, C.J., 2003. Basalt weathering laws and the impact of basalt weathering on the global carbon cycle. Chem. Geol. 202, 257–273.
- Dosseto, A., Bourdon, B., Turner, S.P., 2008. Uranium-series isotopes in river materials: insights into the timescales of erosion and sediment transport. Earth Planet. Sci. Lett. 265, 1–17.
- Drever, J.I., Stillings, L., 1997. The role of organic acids in mineral weathering. Colloids Surf. A 120, 167–181.
- Duff, M.C., Coughlin, J.U., Hunter, D.B., 2002. Uranium coprecipitation with iron oxide minerals. Geochim. Cosmochim. Acta 66, 3533–3547.
- Dupre, B., Dessert, C., Oliva, P., Godderis, Y., Viers, J., Francois, L., Millot, R., Gaillardet, J., 2003. Rivers, chemical weathering and Earth's climate. C. R. Géosci. 335, 1141–1160.
- Engel, J.M., Ma, L., Sak, P.B., Gaillardet, J., Ren, M., Engle, M.A., Brantley, S.L., 2016. Quantifying chemical weathering rates along a precipitation gradient on Basse-Terre Island, French Guadeloupe: new insight from U-series isotopes in weathering rinds. Geochim. Cosmochim. Acta 195, 29–67.
- Fleischer, R.L., 1980. Isotopic disequilibrium of uranium: alpha-recoil damage and preferential solution effects. Science 207, 979–981.

- Gaillardet, J., Dupré, B., Louvat, P., Allègre, C.J., 1999. Global silicate weathering and  $CO_2$  consumption rates deduced from the chemistry of large rivers. Chem. Geol. 159, 3–30.
- Gaillardet, J., Braud, I., Hankard, F., et al., 2018. OZCAR: the French network of critical zone observatories. Vadose Zone J. 17, 180067. https://doi.org/10.2136/vzj2018. 04.0067
- Gaillardet, J., Rad, S., Rive, K., Louvat, P., Gorge, C., Allegre, C.J., Lajeunesse, R., 2011. Orography-driven chemical denudation in the Lesser Antilles: evidence for a new feed-back mechanism stabilizing atmospheric CO2. Am. J. Sci. 311, 851–894.
- Gislason, S.R., Oelkers, E.H., Eiriksdottir, E.S., Kardjilov, M.I., Gisladottir, G., Sigfusson, B., Snorrason, A., Elefsen, S.O., Hardardottir, J., Torssander, P., Oskarsson, N., 2009. Direct evidence of the feedback between climate and weathering. Earth Planet. Sci. Lett. 277 (1–2), 213–222.
- Godsey, S.E., Kirchner, J.W., Clow, D.W., 2009. Concentration-discharge relationships reflect chemostatic characteristics of US catchments. Hydrol. Process. 23, 1844–1864.
- Hall, S.J., Silver, W.L., 2015. Reducing conditions, reactive metals, and their interactions can explain spatial patterns of surface soil carbon in a humid tropical forest. Biogeochemistry 125, 149–165.
- Hawkesworth, C.J., Powell, M., 1980. Magma genesis in the lesser Antilles island arc. Earth Planet. Sci. Lett. 51, 297–308.
- Ivanovich, M., Harmon, R.S., 1992. Uranium-Series Disequilibrium: Applications to Earth. Marine, and Environmental Sciences. Clarendon Press, Oxford.
- Jordan, T.H., 1975. The present-day motion of the Caribbean plate. J. Geophys. Res. 80, 4433-4439.
- Jung, H., Navarre-Sitchler, A., 2018. Scale effect on the time-dependence of mineral dissolution rates in physically heterogeneous porous media. Geochim. Cosmochim. Acta 231, 70-83. https://doi.org/10.1016/j.gca.2018.05.009.
- Krishnaswawi, S., Williams, G.A., Graustein, W.C., Turekian, K.K., 2004. The effect of weathering regime on uranium decay series and osmium in two soil profiles. Geochem. J. 38, 651–660.
- Lebedeva, M.I., Sak, P.B., Ma, L., Brantley, S.L., 2015. Using a mathematical model of a weathering clast to explore the effects of curvature on weathering. Chem. Geol. 404, 88–99.
- Lloret, E., Dessert, C., Gaillardet, J., Alberic, P., Crispi, O., Chaduteau, C., Benedetti, M.F., 2011. Comparison of dissolved inorganic and organic carbon export in the rivers of tropical volcanic island; example from Guadeloupe, French West Indies. Chem. Geol. 280, 65–78.
- Ma, L., 2018. Major element concentrations in weathering rinds and andesitic cores of Basse-Terre Island (French Guadeloupe). Earth Chem. Libr. https://doi.org/10. 1594/IEDA/111220.
- Ma, L., Chabaux, F., Pelt, E., Blaes, E., Jin, L., Brantley, S.L., 2010. Regolith production rates calculated with uranium-series isotopes at Susquehanna/Shale Hills Critical Zone Observatory. Earth Planet. Sci. Lett. 297, 211–225.
- Ma, L., Chabaux, F., Pelt, E., Granet, M., Sak, P.B., Gaillardet, J., Lebedeva, M., Brantley, S.L., 2012. The effect of curvature on weathering rind formation: evidence from Uranium-series isotopes in basaltic andesite weathering clasts in Guadeloupe. Geochim. Cosmochim. Acta 80, 92–107.
- Ma, L., Dosseto, A., Gaillardet, J., Sak, P., Brantley, S.L., 2018. Quantifying weathering rind formation rates by in situ measurements of U-series disequilibria with laser ablation (LA) MC-ICPMS. Geochim. Cosmochim. Acta. https://doi.org/10.1016/j. gca.2018.12.020.
- Maher, K., 2010. The dependence of chemical weathering rates on fluid residence time. Earth Planet. Sci. Lett. 294, 101–110.
- Maher, K., DePaolo, D.J., Lin, J.C.F., 2004. Rates of silicate dissolution in deep-sea sediment: in situ measurement using U-234/U-238 of pore fluids. Geochim. Cosmochim. Acta 68. 4629–4648.
- Maher, K., Steefel, C.I., DePaolo, D.J., Viani, B.E., 2006. The mineral dissolution rate conundrum: insights from reactive transport modeling of U isotopes and pore fluid chemistry in marine sediments. Geochim. Cosmochim. Acta 70, 337–363.
- Navarre-Sitchler, A., Brantley, S., 2007. Basalt weathering across scales. Earth Planet. Sci. Lett. 261, 321–334.
- Nugent, M.A., Brantley, S.L., Pantano, C.G., Maurice, P.A., 1998. The influence of natural mineral coatings on feldspar weathering. Nature 395, 588–591.
- Oelkers, E., Schott, J., 2009. Thermodynamics and kinetics of water-rock interaction. Rev. Mineral. Geochem. 70.
- Pacheco, F.A.L., Alencoao, A.M.P., 2006. Role of fractures in weathering of solid rocks: narrowing the gap between laboratory and field weathering rates. J. Hydrol. 316, 248–265.
- Pelt, E., Chabaux, F., Innocent, C., Navarre-Sitchler, A.K., Sak, P.B., Brantley, S.L., 2008. Uranium-thorium chronometry of weathering rinds: rock alteration rate and paleo-isotopic record of weathering fluids. Earth Planet. Sci. Lett. 276, 98–105.
- Pett-Ridge, J., Monastra Valerie, M., Derry Louis, A., Chadwick, Oliver, 2007. Importance of atmospheric inputs and Fe-oxides in controlling soil uranium budgets and behavior along a Hawaiian chronosequence. Chem. Geol. 244, 691–707. https://doi.org/10.1016/j.chemgeo.2007.07.016.
- Porter, S.C., 1975. Weathering rinds as a relative-age criterion: application to subdivision of glacial deposits in the Cascade Range. Geology 3, 101–104.
- Rosholt, J., Doe, B., Tatsumoto, M., 1966. Evolution of the isotopic composition of uranium and thorium in soil profiles. Geol. Soc. Am. Bull. 77, 987–1004.

- Sak, P.B., Murphy, M., Ma, L., Gaillardet, J., Herdon, E.M., Daniel, C., Brantley, S.L., 2018. From unweathered core to regolith: rates and trends of in situ chemical weathering on tropical volcanic island (Bass Terre Island, French Guadeloupe). Chem. Geol. 498, 17–30.
- Sak, P.B., Navarre-Sitchler, A.K., Miller, C.E., Daniel, C.C., Gailardet, J., Buss, H.L., Lebedeva, M.I., Brantley, S.L., 2010. Controls on rind thickness on basaltic andesite clasts weathering in Guadeloupe. Chem. Geol. 276, 129–143.
- Samper, A., Quidelleur, X., Lahitte, P., Mollex, D., 2007. Timing of effusive volcanism and collapse events within an oceanic arc island: Basse-Terre, Guadeloupe archipelago (Lesser Antilles Arc), Earth Planet, Sci. Lett. 258, 175–191.
- Sarin, M.M., Krishnaswami, S., Somayajulu, B.L.K., Moore, W.S., 1990. Chemistry of uranium, thorium, and radium isotopes in the Ganga-Brahmaputra river system weathering processes and fluxes to the Bay of Bengal. Geochim. Cosmochim. Acta 54, 1387–1396.
- Thompson, A., Rancourt, D., Chadwick, O., Chorover, J., 2011. Iron solid-phase differentiation along a redox gradient in basaltic soils. Geochim. Cosmochim. Acta 75, 119–133.
- Velbel, M.A., 1993. Constancy of silicate-mineral weathering-rate ratios between natural and experimental weathering: implications for hydrologic control of differences in absolute rates. Chem. Geol. 105, 89–99.

- Vigier, N., Bourdon, B., Turner, S., Allegre, C.J., 2001. Erosion timescales derived from U-decay series measurements in rivers. Earth Planet. Sci. Lett. 193, 485–499.
- Vitousek, M.P., Kennedy, M.A., Derry, L., Chadwick, O., 1999. Weathering versus atmospheric sources of strontium in ecosystems on young volcanic soils. Oecologia 121, 255–259. https://doi.org/10.1007/s004420050927.
- Walker, J., Hays, P., Kasting, J., 1981. A negative feedback mechanism for the long-term stabilization of Earth's surface temperature. J. Geophys. Res. 86, 9776–9782.
- Wasklewicz, T.A., 1994. Importance of environment on the order of mineral weathering in olivine basalts, Hawaii. Earth Surf. Process. Landf. 19, 715–734.
- West, A.J., Galy, A., Bickle, M., 2005. Tectonic and climatic controls on silicate weathering. Earth Planet. Sci. Lett. 235, 211–228.
- White, A.F., Brantley, S.L., 2003. The effect of time on the weathering of silicate minerals: why do weathering rates differ in the laboratory and field? Chem. Geol. 202, 479–506.